NH$_3$-promoted hydrolysis of NO$_2$ induces explosive growth in HONO

Wanyun Xu[1], Ye Kuang[2,*], Chunsheng Zhao[3], Jiangchuan Tao[2], Gang Zhao[3], Yuxuan Bian[4], Wen Yang[5], Yingli Yu[3], Chuanyang Shen[3], Linlin Liang[1], Gen Zhang[1], Weili Lin[6], Xiaobin Xu[1]

[1] State Key Laboratory of Severe Weather, Key Laboratory for Atmospheric Chemistry, Institute of Atmospheric Composition, Chinese Academy of Meteorological Sciences, Beijing, 100081, China.

2 Institute for Environmental and Climate Research, Jinan University, Guangzhou, China.

[3] Department of Atmospheric and Oceanic Sciences, School of Physics, Peking University, Beijing, China

[4] State Key Laboratory of Severe Weather, Chinese Academy of Meteorological Sciences, Beijing, 100081, China

[5] State Key Laboratory of Environmental Criteria and Risk Assessment, Chinese Research Academy of Environmental Sciences, Beijing, 100081, China

[6] College of Life and Environmental Sciences, Minzu University of China, Beijing, 100081, China

Corresponding author: Ye Kuang (kuangye@jnu.edu.cn)

Abstract

The study of atmospheric nitrous acid (HONO), which is the primary source of OH radicals, is crucial to atmospheric photochemistry and heterogeneous chemical processes. The heterogeneous NO$_2$ chemistry under haze conditions was pointed out to be one of the missing sources of HONO on the North China Plain, producing sulfate and nitrate in the process. However, controversy exists between various proposed mechanisms, mainly debating on whether SO$_2$ directly takes part in the HONO production process and what roles NH$_3$ and the pH value play in it. In this paper, never before seen explosive HONO production (maximum rate: 16 ppb h^{-1}) was reported and evidence was found for the first time in field measurements during fog episodes (usually with 4<pH<6) and haze episodes under high relative humidity (pH≈4), that NH$_3$ was the key factor that promoted the hydrolysis of NO$_2$, leading to explosive growth of HONO and nitrate under both high and lower pH conditions. The results also suggest that SO$_2$ takes minor or insignificant part in the HONO formation during fog and haze events, but was indirectly oxidized upon the photolysis of HONO through subsequent radical mechanisms. Aerosol hygroscopicity significantly increased with the rapid inorganic secondary aerosol formation further promoting the HONO production as a positive feedback. For future photochemical and aerosol pollution abatement, it is crucial to introduce

34 effective NH₃ emission control measures, since the NH₃-promoted NO₂ hydrolysis is a large
35 daytime HONO source, releasing large amounts of OH radicals upon photolysis, which will
36 contribute largely to both atmospheric photochemistry and secondary aerosol formation.

37

1 Introduction

39   Nitrous acid (HONO) plays a vital role in atmospheric chemistry due to the fact that its
40 photolysis is a major source (Michoud et al., 2014;Kleffmann et al., 2005) of hydroxyl radical (OH)
41 which determines the atmospheric oxidative capacity and plays crucial role in tropospheric
42 chemistry in processes such as the ozone formation, the degradation of volatile organic compounds
43 and the secondary aerosol formation (Cheng et al., 2016;Wang et al., 2016). Hence, the source
44 study of nitrous acid (HONO) is of crucial importance for the understanding of the tropospheric
45 chemistry, for chemistry and climate modelling and for developing effective pollution control
46 strategies (Lu et al., 2018).

47   The North China Plain (NCP) is troubled by the persistent complex air pollution with high
48 loadings of both photochemical pollutants and particulate pollution (Zheng et al., 2015;Ran et al.,
49 2011) and the simultaneous mitigation of the two types of pollution has encountered trouble due
50 to the nonlinear dependence of ozone on NOx (Xing et al., 2018). Unknown daytime sources of
51 HONO caught attention during the past few years (Michoud et al., 2014;Liu et al., 2014;Su et al.,
52 2011) and results from a recent study indicate that an additional missing source is required to
53 explain more than 50% of observed HONO concentration in the daytime in Western China (Huang
54 et al., 2017). Results from several recent studies demonstrate that intense heterogeneous
55 conversion of NO₂ to HONO on particle surfaces might be a significant source of HONO (Cui et
56 al., 2018;Liu et al., 2014).

57   Two main HONO heterogeneous production pathways involving aerosol water and NO_2
58 were proposed. In light of drastic decrease of solar radiation during severe haze events and rich
59 ammonia conditions on the NCP, the first pathway hypothesized that NO_2 (g) dissolved in aerosol
60 water at aerosol pH > 5.5 rapidly formed HONO while oxidizing HSO_3^- (aq) to sulfate. The
61 stoichiometry of this mechanism is as follows (Cheng et al., 2016;Wang et al., 2016):

62         $2NO_2$ (aq) + HSO_3^- (aq) + H_2O (l) ➜ $2H^+$ + HSO_4^- (aq) + $2NO_2^-$ (aq).   (R1)

63   Based on this mechanism, good agreement between modelled and observed sulfate

64   formation rates were achieved. However, the assumption that the pH of ambient aerosols can reach

65   beyond 5.5 is a debatable issue. Results from several most recent studies indicate that the pH of

66   ambient aerosols fall in the range of 3-5 in most cases (Ding et al., 2018;Liu et al., 2017a;Song et

67   al., 2018). Given this, it was proposed that HONO and NO_2^- were produced in the hydrolysis

68   process of NO_2, releasing OH radicals upon photolysis, which indirectly oxidize SO_2 to sulfate (Li

69   et al., 2018b):

70            $2NO_2$ (g) + H_2O (l) ➡ H^+ + NO_3^- (aq) + HONO. (R2)
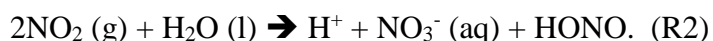
71   Results of Yabushita et al. (2009) suggest that anions (such as Cl^-, Br^- and I^-) greatly

72   enhance the hydrolysis of NO_2 on water, and the NO_2 uptake coefficients of R2 can be enhanced

73   several orders of magnitude by increasing electrolyte concentration. The ambient aerosol particles

74   in the boundary layer are in aqueous phase under high RH (Liu et al., 2017b) and the aerosol or

75   fog water is not pure with different dissolved anions (Wu et al., 2018;Lu et al., 2010). Therefore,

76   HONO and nitrate formed through this mechanism should be independent of aerosol acidity, and

77   should be primarily affected by the aerosol surface area density (S_a), aerosol liquid water content

78   and NO_2 concentration (Li et al., 2018b). Moreover, recent theoretical simulations have proposed

79   a HONO formation mechanism involving NO_2 and water and have identified that NH_3 can promote

80   the hydrolysis of NO_2 (Li et al., 2018a) (R2). Despite of this, no direct evidence from field

81   observations were available in this paper to support their findings.

82   Although the proposed HONO formation mechanisms are all heterogeneous reactions of

83   NO_2, the details of how SO_2, pH and NH_3 are involved in heterogeneous formation are still under

84   debate (Li et al., 2018b) and a clear mechanism is still missing in current models to explain both

85   the daytime concentration of observed HONO and the secondary inorganic aerosol formation.

86   Measurements of HONO are rare and simultaneous observations of HONO and aerosol physical

87   and chemical characteristics are lacking to thoroughly analyze or directly support the aerosol

88   heterogeneous HONO formation mechanisms involving NO_2. In this paper, we present f

89   simultaneous measurements of HONO, sulfate and nitrate as well as other precursor gases,

90   oxidants and meteorological parameters during both fog and haze episodes under high ambient

91   RH. Fog water pH is usually greater than 5.5 in eastern China (Safai et al., 2008;Lu et al., 2010),

92   while calculations in this work and previous studies collectively indicate a moderately acidic

condition (4<pH<5) for fine particles in northern China winter haze. The observational results unveil that NH_3 is the key factor that promotes the hydrolysis of NO_2, resulting in explosive formation of HONO, nitrate and sulfate.

2 Site description and instruments

From 15th Oct. to 25th Nov. 2016, a field campaign intended to study sulfate formation was conducted at the Ecological and Agricultural Meteorology Station ($39°09′N, 115°44′E$) of the Chinese Academy of Meteorological Sciences. The site is partly composed of experimental farmland and is also surrounded by farmland and small residential towns (nearest town ~1.5 km). It is located between Beijing (~ 100km) and Baoding (~40km), two megacities on the North China Plain (Fig. 1). During this field campaign, an In situ Gas and Aerosol Compositions Monitor (IGAC, Fortelice International Co.,Taiwan) was used for monitoring water-soluble ions (Na^+, K^+, Ca^{2+}, Mg^{2+}, NH_4^+, SO_4^{2-}, NO_3^-, NO_2^-, Cl^-) of PM2.5 (particulate matter with aerodynamic diameter less than 2.5 µm) and trace gases including HONO, SO_2, NH_3, HCl, and HNO_3 with a time resolution of 1h. The IGAC system draws in ambient air through a PM10 inlet and passes the sample through a sharp-cut PM2.5 cyclone at a flowrate of 16.7 L min^{-1}. The total length of the stainless steel sampling line is approximately 2 m, with an inner diameter of 3.18 cm (1.25 inch), resulting in a residence time below 6 s, suggesting that underestimates in NH_3 possibly caused by adsorption on the stainless steel sampling tube as was proposed by Young et al. (2016) might be unimportant. A vertical annular denuder wetted with dilute H_2O_2 solution ($5x10^{-3}$ M) collects the trace gases and converts SO_2 rapidly to SO_4^{2-}, preventing SO_2 from reacting with NO_2 in the absorption solution to produce HONO artefacts. A scrub and impact aerosol collector under the denuder is mounted at an inclined angle to capture particles based on impaction after condensation growth. Two separate Ion Chromatographs are used to respectively analyze anions and cations for the gas and aerosol liquid extracts which were injected from the denuder and the aerosol collector once an hour. The detection limits are below 0.12 μg m^{-3} and the background concentration of most water-soluble inorganic ions within the instrument were below 0.11 μg m^{-3}, only with SO_4^{2-} showing a background concentration of 1.10 μg m^{-3} (Young et al., 2016). Considering the severe pollution state the NCP is under, these measurement uncertainties are fully acceptable. The instrument has shown good performance in the past, agreeing well with filter based samples (Liu et al., 2017a). Standard LiBr solution was continuously added to the aerosol liquid extracts during

123 the measurements, to ensure the sampling and analyzing process is stable. The swing amplitude

124 was within the range of three standard deviation, confirming the stability of the ion analyzing

125 system throughout the campaign. A mixed standard solution was diluted to perform multipoint

126 calibrations (at 5, 10, 20, 50, 100, 200, 500 and 1000 ppb concentrations) at the beginning and at

127 the end of the campaign for the ions Na^+, K^+, Ca^{2+}, Mg^{2+}, NH_4^+, Li^+, SO_4^{2-}, NO_3^-, NO_2^-, Cl^-, Br^-,

128 with the R^2 of the calibrations reaching above 0.9999. A comparison between NH_3 observed by

129 IGAC and by an economical NH_3 analyser (LGR, DLT-100, details see Meng et al. (2018)) yielded

130 an overall slope of 0.91 with R=0.63 (Fig.S1a). A better comparison result (slope of 1.03, R=0.74)

131 would be obtained if data associated with RH≥80 were excluded (Fig.S1b). The overestimation of

132 LGR instruments compared to denuder based instruments has also been reported in Teng et al.

133 (2017), suggesting possible interference of water vapor on NH_3 measurements. As can be seen in

134 Fig.S2, both instruments captured the same the diurnal variation of NH_3 during the four case

135 episodes in this study, which proves that the IGAC instrument was able to capture the overall

136 variation trends of NH_3. Since both instruments have their uncertainties, we decided to use the

137 NH_3 measured by the IGAC instrument for better consistency with the other data.

138   NOx and CO were observed using commercial instruments from Thermo Electronics

139 (Model 42CTL and 48CTL), while the Aerolaser AL2021 H_2O_2-monitor was used to measure

140 H_2O_2 concentrations. The NO_x instrument uses a Mo-based converter, which would result in

141 interference of NO_z species (e.g. HONO, HNO_3, PAN, etc.) on NO_2. Here, we define

142 $NO_2^*=NO_{2,meas}$-HONO-HNO_3, and use it to approximate the true NO_2 concentration. The ambient

143 RH, temperature, wind speed and wind direction were observed using an automatic weather station.

144 The dry state particle number size distributions (PNSDs) in the diameter range of 3nm to 10μm,

145 were jointly measured by a scanning mobility particle size spectrometer (SMPS) and an

146 Aerodynamic Particle Sizer (APS, TSI Inc., Model 3321). The ambient aerosol liquid water

147 concentrations were calculated based on measurements of a three-wavelength humidified

148 nephelometer system (Kuang et al., 2018). The aerosol hygroscopicity parameter κ (Petters and

149 Kreidenweis, 2007) is calculated using the method proposed by Kuang et al. (2017). The aerosol

150 surface area concentration (S_A) is calculated based on measured PNSD and the retrieved

151 hygroscopicity parameter κ based on measurements of the humidified nephelometer system.

3 Observed simultaneous rapid increase of HONO, nitrate and sulfate

The time series of HONO, sulfate, nitrate and ammonium and precursor gases, meteorological parameters and other parameters are shown in Fig. 2. During this observation period, HONO concentration ranged from 0.31 to 17.6 ppb (ranged from 0.3 to 6.0 ppb during most periods) with an average of 3.0 ppb. NO_2^* concentration ranged from 7.1 to 56.3 ppb with an average of 28.9 ppb. NH_3 concentration ranged from 0.05 to 30 ppb with an average of 12.3 ppb. The HONO/NO_2^* ratio ranged from 0.02 to 0.6 with an average of 0.11, which is moderately higher than the previously reported results in Eastern China (Cui et al., 2018;Liu et al., 2014). This is because compared to their measurements, the $PM_{2.5}$ mass concentrations and S_a in this study are much higher (As shown in Fig.3). Additionally, HONO/NO_2^* increases with $PM_{2.5}$ and S_a, which is consistent with previous results, suggesting that aerosol might have promoted the conversion from NO_2 to HONO. In Cui et al. (2018), under the observed $PM_{2.5}$ range of 0 to 100 $\mu g\ m^{-3}$, HONO/NO_2 ranged from 0.0013 to 0.17, with an average of 0.062, while in this study the average HONO/NO_2^* also increases from 0.06 to 0.07 for the same $PM_{2.5}$ range. Liu et al. (2014) reported that average HONO/NO_2 increased from 0.04 to 0.1 when S_a increased from 200 to 1100 $\mu m^2\ cm^{-3}$, while, the average HONO/NO_2^* in this study increased from 0.05 to 0.15 for the same S_A range. The comparison suggests that our HONO measurements were comparable to those made using other instruments previously reported in Eastern China. Further, it can be noticed that for the relatively lower $PM_{2.5}$ concentration and S_A range, HONO/NO_2^* increased rapidly with increasing aerosol loading, while after a critical concentration ($PM_{2.5}$>225 $\mu g\ m^{-3}$, S_a>1100 $\mu m^2\ cm^{-3}$) the increase came to a halt. This indicates that under relatively cleaner conditions, the heterogeneous conversion of NO_2 to HONO might have been limited by aerosol surface area density. However, under severe haze pollution or foggy conditions with sufficient S_a available for heterogeneous reactions, the HONO formation was not sensitive to the change in S_a anymore.

Four rapid HONO formation events were identified in Fig.2, two under foggy conditions and the other two under severe haze with high RH conditions. In the following Sect. 3.1 and 3.2, the variations of the pollutants connected to HONO formation during the four cases will be described in detail, so that the mechanism behind such rapid HONO production under conditions when HONO formation was not sensitive to S_A can be better discussed in Sect. 4.

3.1 Explosive growth of HONO during fog episodes

Two dense fog episodes with rapid HONO increase were observed for the first time in China, occurring on the 4th and 5th Nov. 2016. From satellite images (Fig. 1) it can be seen that on the 5th Nov., a wide area of the NCP was shrouded by fog before noon (about 11:30) including the observation site, however, the fog area reduced in the afternoon (about 13:30) and dissipated near the observation site. The evolution of the fog-shrouded area during these two days was also observed by a geostationary satellite (http://www.eorc.jaxa.jp/ptree/index.html). These two fog episodes offer us a great opportunity to study the hydrolysis process of NO_2 (R2) and the role of SO_2 in heterogeneous HONO production in fog water (R1), which usually show pH above 5.5 (Safai et al., 2008;Lu et al., 2010).

The time series of simultaneously observed meteorological parameters, concentrations of nitrate, ammonium, sulfate and their precursor gases SO_2, NO_2^*, NO and NH_3, as well as atmospheric oxidants such as O_3, H_2O_2 and other parameters including CO, which is indicative of transport processes during the two days with fog episodes are shown in Fig. 4. From 0:00 (Beijing local time) on the 4th Nov., the ambient RH continuously increased and reached 100% near 5:00, and lasted about 8.5 hours before it dropped below 100% near 13:30. However, at 15:30, the ambient RH began to rise again and reached 100% near 19:30, and then sustained until 12:00 on the 5th Nov. The latter fog episode lasted about 18.5 hours.

During the first fog episode, the rapid increases of HONO, nitrate, sulfate and ammonium were observed from 8:50 to 11:30 (Case1). HONO increased from 3.6 ppb to 10.6 ppb, with the most rapid increase occurring around 11:00 at a rate of 5.5 ppb h^{-1}. During the HONO increasing period, the variation characteristics of related trace gases and other parameters are as follows. NH_3 concentration increased slowly at first and then increased drastically near 11 am (10 ppb h^{-1}). SO_2 concentration remained almost constant at first and then increased from near 0.25 ppb to 0.4 ppb. NO_2^* concentration varied little but decreased when HONO was increasing, while NO concentration increased first and then decreased. H_2O_2 concentration is continuously increasing, but O_3 concentration remained near zero. CO concentration remained almost constant (~2.5 ppm), suggesting that there was no evident plume transport during this process. Wind speed was less than 2 m s^{-1}, and dropped almost to 0 m s^{-1} when HONO concentration dramatically increased, further supporting the fact that the drastic increase was not caused by transport processes. Ammonium, nitrate and sulfate concentration steadily increased from 7.5, 13.2, 13.7 μg m^{-3} to 14.3, 30.4,

212 31.0 µg m^{-3}, respectively. A noticeable increase in nitrite was also observed, when HONO

213 increased most rapidly. It should be noted that the cutting diameter of the IGAC instrument is 2.5

214 µm, which means that observed concentrations only represent the variation of inorganics ions in

215 aerosol water, and that of fog droplets were not included.

216   During the second fog episode, HONO, nitrate, sulfate and ammonium started to increase

217 rapidly from 9:30 and reached a plateau near 12:30, when the fog started to dissipate (Case2).

218 HONO increased from 3 ppb to 9.5 ppb, with the fastest increase occurring near 11:00 at a rate of

219 3.5 ppb h^{-1}. NH_3 concentration increased steadily from 5 ppb to 24 ppb. SO_2 concentration

220 increased steadily from 0.25 ppb to 1.25 ppb. NO_2^* concentration decreased continuously at the

221 very beginning (near 40 ppb) and then increased slightly, while NO concentration remained almost

222 constant (near 30 ppb) throughout the entire fog period. H_2O_2 concentration increased slightly at

223 first and then rose rapidly towards the end of the fog period. O_3 concentration increased very

224 slightly. CO concentration remained also near constant (~3 ppm). Wind speed was steadily below

225 2 m s^{-1} at the beginning, however, began to increase quickly at noon. Ammonium, nitrate and

226 sulfate concentration grew steadily from 8.1, 17, 3.8 µg m^{-3} to 15.3, 39.3, 8.0 µg m^{-3}, respectively.

227 The variation of nitrite was very similar to that of HONO. The variation of wind speed

228 demonstrated that at the very beginning of the HONO increase, the air mass was relatively stagnant,

229 but became more turbulent upon the fog dissipation.

3.2 Explosive growth of HONO during haze episodes with high RH conditions

231   Two episodes with rapid HONO increase under severe haze with high RH conditions

232 occurred on the 11th and 14th Nov., respectively. The time series of simultaneously observed

233 meteorological parameters, concentrations of nitrate, ammonium, sulfate and their precursor gases

234 SO_2, NO_2^*, NO and NH_3, as well as oxidants including O_3, H_2O_2 and other parameters such as CO

235 concentration, aerosol volume concentration in dry state and aerosol liquid water content during

236 the two days are shown in Fig.5.

237   On the 11th Nov., HONO started rising from 6:30 (3.4 ppb) and came to a halt at 9:00 (11.5

238 ppb) (Case 3). The quickest increase of HONO occurred near 9 o'clock with a rate of 5.6 ppb h^{-1}.

239 The ambient RH decreased rapidly (from foggy condition to near 75%). NH_3 increased slowly at

240 first and then grew rapidly. NO_2^* decreased slowly and SO_2 remained low. The total volume

241 concentration of $PM_{2.5}$ was decreasing. Ammonium, nitrate and sulfate concentrations increased

very slowly at first and then evident increase was observed in ammonium and nitrate. The decrease in dry state volume concentration of $PM_{2.5}$ demonstrate that the air mass is not quite steady due to transport or boundary layer processes. The slight increase of nitrate and sulfate despite the drop in total $PM_{2.5}$ concentration suggest that the nitrate and sulfate produced during the increasing process of HONO outgrew those lost to boundary layer mixing and transport.

On the 14th Nov., HONO increased drastically near 11:00, reaching 17.6 ppb at 11:30 (16.1 ppb h[-1]) and then dropped promptly to 4 ppb at 12:30 (Case 4). This phenomenon took place when the fog dissipated and the ambient RH abruptly dropped to near 85%. Key variation features of other parameters are as follows. NH_3 increased rapidly from 9.7 ppb to 30 ppb. $NO_2{}^*$ concentration was decreasing when HONO quickly increased, while SO_2 concentration remained low. The concentration of sulfate and nitrate also increased quickly. Volume concentration of $PM_{2.5}$ was decreasing, indicating that even more sulfate and nitrate were formed than the observed growth in their concentrations. The photolysis of HONO was high probably the cause for its drastic decrease. Note that the HONO was not increasing during the period where only $NO_2{}^*$ increased rapidly and NH_3 varied little.

4 Discussions

4.1 HONO budget analysis

In these four rapid HONO increasing episodes, the maximum HONO growth rates (d[HONO]/dt) all exceed 5 ppb h[-1], and even reach beyond 16 ppb h[-1]. Such high HONO growth rates as observed in this study were not yet reported in literature. In this section, we perform a budget analysis by estimating the net HONO production accounting for currently known sources and sinks and by comparing it to observed dHONO/dt. Thereby we can discuss whether the observed HONO formation events can be explained by currently known mechanisms and try to identify which mechanisms are determining the variation of HONO.

The net HONO production rate can be estimated by accounting for all the currently known sources and sinks using the following equation (Huang et al., 2017;Zhang et al., 2019) :

$$P_{HONO}^{net} = P_{emi} + P_{hom}^{net} + P_{het} - L_{pho} - L_{dep}, \quad\quad\quad (\text{Eq.1})$$

where P_{emi} is the total emission rate of HONO, P_{hom}^{net} the net HONO production in homogenous gas phase reactions, P_{het} the HONO produced via heterogeneous reactions, L_{pho} the loss of HONO due to photolysis and L_{dep} the loss of HONO due to deposition.

272   Previous studies have shown that HONO can be emitted through biomass burning and

273   vehicles (Nie et al., 2015;Huang et al., 2017). Biomass burning contributes to HONO mainly by

274   increasing S_a and NO_2 conversion efficiency (Nie et al., 2015). Under foggy conditions, surface

275   area was not the limiting factor to the NO_2 conversion. During the haze events, S_a was decreasing

276   due to decreasing humidity and aerosol water content. Hence, the variation of surface area cannot

277   explain the observed HONO increases. According to the mapped fire spots on the days of the

278   HONO events (Fig.S3), there was no fire within 20 km distance to the site. K^+ is often used as an

279   indicator for biomass burning. The average K^+ concentration during the whole campaign ranged

280   from 0.022 to 5.95 μg m^{-3}, with an average of 1.28 μg m^{-3}. The K^+ level during the four events

281   were 1.39, 1.08, 1.51 and 1.54 μg m^{-3}, respectively, showing no evident sign of biomass burning.

282   Hence, only vehicle emissions were considered in this study.

283   Vehicle emissions can be estimated using the following equation:

284    $P_{vehicle} = R_{emission} \times [NO_x]_{vehicle},$ (Eq.2)

285   where $R_{emission}$ is the vehicle emission ratio and $[NO_x]_{vehicle}$ the NO_x concentration from vehicle

286   emissions. The NO/NO_x ratio during the HONO increasing episodes ranged from 0.37 to 0.76,

287   suggesting that the air masses were relatively aged compared to freshly emitted air mass from

288   exhaust (NO/NO_x>0.9). Here, $P_{vehicle}$ is estimated assuming all the measured NO_x came from

289   vehicle emissions and an emission ratio of 1%, which is higher than the upper limit of 0.8% used

290   in Huang et al. (2017), to obtain an upper limit for vehicle emissions.

291   HONO can be formed in gas phase reactions of NO with OH radicals and is lost through

292   direct reactions with OH radicals. The net production of HONO via homogeneous reactions can

293   be estimated using the equation:

294    $P_{hom}^{net} = k_{NO+OH}[NO][OH] - k_{HONO+OH}[HONO][OH],$ (Eq. 3)

295   where k_{NO+OH} (7.2×10^{-12} cm^{-3} s^{-1}) and $k_{HONO+OH}$ (5.0×10^{-12} cm^{-3} s^{-1}) are the rate constants of

296   the reactions of NO and HONO with OH, at 298 k, respectively (Li et al., 2012). The diurnal

297   variation of OH concentrations was inferred from Whalley et al. (2015), replacing OH under fog

298   conditions with 1x10^5 cm^{-3} (Fig.S4).

299   Heterogeneous conversion of NO_2 on aerosol and ground surface is considered a major

300   source for HONO. However, the detailed mechanism (R1 or R2?) is still under debate and different

301   studies have shown a large variability in the range of estimated NO_2 uptake coefficient. Typically,

302   the conversion of NO_2 on aerosol and ground surface is parameterized as a linear function of NO_2

303   uptake coefficients and surface to volume ratios (or S_a) (Xue et al., 2014;Li et al., 2018b):

304     $P_{het} = (k_g + k_a)[NO_2^*],$ (Eq.4-1)

305     $k_g = \frac{1}{8} \cdot \vartheta_{NO2} \cdot \gamma_g \cdot \frac{S}{V},$ (Eq.4-2)

306     $k_a = \frac{1}{4} \cdot \vartheta_{NO2} \cdot \gamma_a \cdot S_a,$ (Eq.4-3)

307   where ϑ_{NO2} stands for the mean molecular speed, γ_g and γ_a for the uptake coefficient on ground

308   and aerosol surface, S/V for the surface to volume ratio and S_a for the ambient aerosol surface area

309   density. For NO_2 conversion on ground surface, γ_g is assumed to be 1×10^{-6} and S/V is assumed

310   to be 0.1 m^{-1} (Li et al., 2010;Xue et al., 2014;Vogel et al., 2003). Since no measurements of fog

311   droplet surface areas were made in this experiment, estimates for NO_2 conversion under foggy

312   conditions could not be incorporated. For non-fog conditions, the ambient S_a calculated using the

313   simultaneously measured PNSD and aerosol hygroscopicity parameter derived from

314   measurements of a humidified nephelometer system were applied to further calculate the variation

315   of the HONO production on aerosol surface. Here, with an overall consideration of the γ_a used in

316   past literature (Li et al., 2010;Xue et al., 2014;Li et al., 2018b), γ_a was assumed to be $5\times10^{-6}, 2\times10^{-4}$

317   and $2\times10^{-4}\times$(solar radiation/400) for nighttime, daytime with solar radiation below and above

318   400 Wm^{-2}, respectively, to account for both anion-enhanced and photo-enhanced NO_2 conversion.

319   HONO loss through photolysis reactions were calculated as:

320     $L_{pho} = J_{HONO}[HONO],$ (Eq.5)

321   where JHONO was modelled using the TUV radiative transfer model (version 5.3,

322   http://www2.acom.ucar.edu/modeling/tuv). The required single scattering albedo and aerosol

323   angstrom exponent were estimated using simultaneously measured PNSD and BC measurements

324   (Kuang et al., 2015), while the 550nm aerosol optical depth (AOD) was assumed to vary with RH

325   (Table S1).

326   Loss through dry deposition was estimated using equation 6:

327     $L_{dep} = \frac{v_{dep}}{H}[HONO],$ (Eq.6)

328   where the dry deposition rate v_{dep} was assumed to be 0.3 cm s^{-1} according to (Stutz et al., 2002)

329   and the boundary layer height H was interpolated from ECWMF ERA-interim data

330   (http://apps.ecmwf.int/datasets/data/interim-full-daily/).

331   The comparison between the calculated HONO net production rate and actually measured

332   HONO variation rate (d[HONO]/dt) is displayed in Fig. 6. The estimated upper limit for vehicle

333   emissions displays little variability during the day, with slight decreasing trends during the four

334   events, proving that the observed HONO production could not have been caused by direct vehicle

335   emissions. The net gaseous phase production of HONO (P_{hom}^{net}) contributed 0.15-0.18, 0.04-0.07,

336   0.27-1.04 and 0.25-1.53 ppb h^{-1} during the 4 case events, displaying little influence during fog

337   events and more during haze events. However, the estimated P_{hom}^{net} was far from sufficient to

338   explain the observed d[HONO]/dt. Dry deposition was typically high during the night within the

339   shallow nocturnal boundary layer and decreased during the day with the increase of the boundary

340   layer height. The calculated L_{dep} contributed 0.5-0.9, 0.4-0.6, 2.7-4.3 and 0.05-0.3 ppb h^{-1} to the

341   loss of HONO. No significant decreases in L_{dep} were observed during the two fog events, while

342   increases were detected during the cases on 11th and 14th Nov. Not only was the variation in L_{dep}

343   unable to explain observed HONO productions, it further added to the discrepancy between

344   observed and calculated d[HONO]/dt. During the four case events the J_{HONO} respectively increased

345   from 0.7×10^{-4} to 2.5×10^{-4} s^{-1}, 1.6×10^{-4} to 2.4×10^{-4} s^{-1}, 0.03×10^{-4} to 1.4×10^{-4} s^{-1} and 1.6×10^{-4} to

346   4.4×10^{-4} s^{-1}, with L_{pho} contributing 0.9-8.9, 2.2-7.8, 0.03-5.5 and 0.8-26.4 ppb h^{-1} to the loss of

347   HONO. J_{HONO} increased significantly by the end of the HONO growth events to 2.9×10^{-4}, 4.3×10^{-4},

348   2.6×10^{-4} and 6.6×10^{-4} s^{-1}, respectively, suggesting that the rapid drop of HONO concentrations

349   was high probably caused by the rapid photolysis. Overall, L_{pho} contributed most to the discrepancy

350   between observed and calculated d[HONO]/dt.

351   Generally, the observed and calculated d[HONO]/dt agreed better with each other outside

352   the HONO explosive growth periods, showing overestimations when S_A was high. For the fog

353   cases, no S_A was available to account for P_{het}, however, for the haze case on 11th Nov (Fig. 6c) it

354   can be noted that by accounting for the photo-enhanced NO$_2$ conversion, an overestimation in P_{het}

355   occurred between 14 to 18 LT, while the rapid HONO formation in the morning could not be

356   explained. This further suggests that the observed discrepancies in HONO production have mainly

357   been caused by uncertainties in the heterogeneous formation (NO$_2$ uptake coefficient) estimates.

358   The fact that HONO drastically increased while NO$_2$ varied little (9:30 to 11:30, 5th Nov. and 6:30

359   to 8:30, 11th Nov.) or hardly increased even under drastic increases of NO$_2$ (8:30 to 11:30, 14th

360   Nov.), but displayed explosive growth with increasing NH$_3$, could not be explained by currently

361   known HONO sources (direct emission or gas phase reactions). Additionally, these rapid

362 increasing HONO phenomena were all observed under foggy or severe haze with high RH

363 conditions, which further affirms the suspicion that the HONO increase was caused by

364 heterogeneous conversion of NO_2. Under such conditions, S_A was not the controlling factor

365 determining the conversion of NO_2, so which mechanism could have been behind such rapid

366 HONO production?

4.2 Heterogeneous HONO formation mechanism

368 As manifested in Sect. 4.1, the unknown HONO source and the overestimates in HONO

369 production were both linked to our limited understanding on the heterogeneous HONO formation

370 mechanism. In this section, we try to evaluate the relative contribution of the currently known

371 heterogeneous HONO formation pathways (R1 and R2) and reveal the reason for their limitations

372 in explaining the observed HONO growth.

373 To evaluate which process (R1 or R2) was dominating the heterogeneous production of

374 HONO, we assume that HONO was produced in aerosol and fog water simultaneously via R1 and

375 R2. Since measurements of fog liquid water content or fog droplet surface area density were not

376 made, we cannot directly quantify the absolute HONO production in fog. However, we can make

377 a few assumptions to compare the relative HONO contribution via R1 and R2. First, it was

378 assumed that the observed sulfate production (d[SVI]/dt) was caused by the reaction of SO_2 with

379 H_2O_2, O_3, NO_2, transition metal ions (TMI: Fe^{3+} and Mn^{2+}). Calculations were performed

380 according to Cheng et al. (2016), using the same pH dependent TMI concentrations and the

381 actually measured SO_2, H_2O_2, O_3 and NO_2^* concentrations (Table S2). For the two fog episodes

382 on 4th and 5th Nov. 2016, the mean diameter of fog droplets was assumed to be 7.0 μm and the

383 liquid water content was assumed to be 0.3 g m^{-3} according to Shen et al. (2018). For the haze

384 episodes on the 11th and 14th Nov. 2016, the mean aerosol diameter under ambient conditions was

385 estimated to be 0.65-1.22 and 0.9 μm (size-resolved volume contribution of aerosol particles in

386 dry state peaks near 500 nm), while the liquid water content was calculated to decrease from

387 5.7×10^{-4} to 6.4×10^{-5} g m^{-3} on the 11th Nov and assumed to be 0.01 g m^{-3} on the 14th Nov. during

388 the transition from fog to haze. The sulfate production rate and relative contribution of each

389 oxidation pathway to the total sulfate production rate was obtained and depicted in Fig.7. For the

390 two fog episodes, assuming pH=6, the estimated average sulfate production rates are 16.6 and 49.1

391 μg m^{-3} h^{-1}, respectively, approximately 3 and 7 times of that observed within $PM_{2.5}$, which might

392 be an underestimation, considering the liquid water content of fog droplets are at least a magnitude

393 higher than that of aerosols. For the two haze episodes, using the pH values estimated using

394 ISORROPIA (forward mode and metastable assumption (Song et al., 2018)), the estimated average

395 sulfate production rates are 0.12 and 0.88 µg m^{-3} h^{-1}, about 14% and 19% of that observed within

396 PM$_{2.5}$. Following the calculations of Cheng et al. (2016), we have considered the influence of ionic

397 strength on the reaction rates and set constraints on the maximum ionic strength (I_{max}), which might

398 have caused underestimations for all reaction routes, since the calculated ionic strength commonly

399 exceeded I_{max}. Underestimated transition metal ion concentrations may also be partly responsible

400 for the underpredicted sulfate production, since the TMI catalysis route has recently be pointed out

401 to be the dominant SO$_2$ heterogeneous oxidation pathway (Shao et al., 2019) under low pH

402 conditions. Additionally, there also might be other neglected SO$_2$ oxidation pathways, which will

403 lead to overestimates in the sulfate fraction produced by the NO$_2$ oxidation pathway. Therefore,

404 we can only yield an upper limit for the HONO production rate of R1:

405 $$\frac{d[HONO]}{dt}\bigg|_{R1} = 2 \times frac_{SO_2+NO_2} \times \frac{d[SVI]}{dt}\bigg|_{obs}, \qquad\qquad (Eq.7)$$

406 where $frac_{SO_2+NO_2}$ is the contribution fraction of the NO$_2$ oxidation pathway to the total sulfate

407 production. Note that the calculated HONO production rate can only represent the production

408 within PM$_{2.5}$.

409 By further assuming that all the observed HNO$_3$ and nitrate production (d[HNO$_3$+NO$_3^-$]/dt) was

410 caused by reaction R2 and by the reaction of NO$_2$ with OH radicals (k_{NO_2+OH}=3.2×10^{-12} cm^3 s^{-1}),

411 the HONO production rate of R2 would be:

412 $$\frac{d[HONO]}{dt}\bigg|_{R2} = \frac{d[HNO_3+NO_3^-]}{dt}\bigg|_{obs} - k_{NO_2+OH}[NO_2^*][OH]. \qquad\qquad (Eq.8)$$

413 The contribution fraction of the two reactions to the heterogeneous HONO production in aerosol

414 and fog liquid water content can be calculated by:

415 $$f_{R1} = \frac{d[HONO]}{dt}\bigg|_{R1} \bigg/ \frac{d[HONO]}{dt}\bigg|_{R1+R2} \quad \text{and} \qquad\qquad (Eq.9-1)$$

416 $$f_{R2} = \frac{d[HONO]}{dt}\bigg|_{R2} \bigg/ \frac{d[HONO]}{dt}\bigg|_{R1+R2}. \qquad\qquad (Eq.9-2)$$

417 Assuming the pH of fog droplets falls within the range of 4 to 6, f_{R2} was estimated to range

418 from range from 79.4 to 99.6% and from 85.5 to 99.6% during the 4th and 5th Nov. 2016,

419 respectively. For the two haze events on 11th and 14th Nov., the f_{R2} corresponding to the pH values

420 modelled by ISORROPIA would be 99.2% and 99.9%.

421   These results suggest that, reaction R2 is the dominant contributor to the heterogeneous

422 HONO production, while R1 is more important under high pH conditions. Under the assumed

423 upper limit of pH, R1 could have contribute up to 20.6% and 14.5% to the observed HONO growth

424 during the two fog events. This is in accordance with results from Wang et al. (2016) and Cheng

425 et al. (2016), which suggested that R1 was more likely to happen during fog episodes or under

426 NH_3 neutralized conditions (3,4). For the two haze events, R1 contributed very little (0.8% and

427 0.1%) to the observed HONO growth.

428   Since R2 seems to be the dominant contributor to the observed HONO production, it is

429 important to evaluate whether the parameterizations in current literature can accurately describe

430 the HONO production process of R2. The HONO production rate of R2 is typically parameterized

431 as in Eq.4, where the NO_2 reactive uptake coefficient, NO_2 concentration and the surface area

432 density of fog droplets/aerosol particles are the controlling factors of the NO_2 uptake, as opposed

433 to the pH of the water droplets (Li et al., 2018b;Yabushita et al., 2009). Based on the NO_2 reactive

434 uptake coefficient (γ_{NO_2}) range of 1×10^{-4} to 1×10^{-3} in Yabushita et al. (2009) and Li et al. (2018b),

435 which is represents the upper limit for currently reported γ_{NO_2}, we have calculated the HONO

436 production rate of R2 under different conditions (Fig.S5). During foggy conditions, the HONO

437 production rate would be higher than 1 ppb (ppb $NO_2\cdot$h)$^{-1}$. NO_2^* during the two fog episodes

438 ranged between 37 to 40 ppb, therefore, the HONO production rate would have been higher than

439 40 ppb h^{-1}. However, no rapid increase of HONO was observed unless NH_3 was simultaneously

440 increasing. The same conclusion can be reached for hazy conditions. If we had used a constant

441 γ_{NO_2} of 1×10^{-4} for hazy conditions in the budget analysis, the calculated P_{het} would significantly

442 overestimate the HONO production when relative humidity was high and large ambient S_a were

443 observed, while it would fail to reproduce the growth in HONO on the morning of the 11th Nov.

444 2016 (Fig. S6). The γ_{NO_2} parameterization in Sect. 4.1, which accounted for photo-enhancement,

445 also failed to explain the morning growth of HONO and resulted in overestimated HONO

446 production during the afternoon. These results indicate that γ_{NO_2} is not a constant, the currently

447 proposed γ_{NO_2} parameterization schemes for R2 are missing the important impact of NH_3. The

448 γ_{NO_2} range used in Yabushita et al. (2009) and Li et al. (2018b) highly overestimated HONO

449 production, when NH_3 was not abundant enough, while it was insufficient to explain the observed

450 HONO production with the growth of NH_3.

451 Recent theoretical simulation results ascertain that NH_3 can promote the hydrolysis of NO_2

452 and contribute to HONO formation via R2 by reducing the free energy barrier of the reaction and

453 stabilizing the product state (Li et al., 2018a). This conclusion is consistent with the observed

454 phenomena that HONO only increased rapidly when NH_3 was simultaneously increasing.

455 Considering the influence of NH_3 and sulfate on the aerosol pH, under our observed NH_3

456 concentration range, NH_3 has negligible impact on pH values (Guo et al., 2017), especially under

457 high RH conditions. This further proves that the NH_3-promoted hydrolysis of NO_2 is independent

458 of the pH value. Another phenomenon worth noting is that, in Case 3, HONO was increasing

459 rapidly even under the drastic decrease in ambient RH, which demonstrates that the impact of NH_3

460 on HONO formation should be even more important than that of aerosol liquid water content.

461 However, the hydrolysis of NO_2 needs water to be involved, thus, the importance of water content

462 under different conditions remains to be elucidated.

463 To further investigate the acceleration effect of NH_3 on the hydrolysis of NO_2, we have

464 examined the correlations between the NO_2^*-to-HONO (HONO/ NO_2^* ratio), NO_2^*-to-NO_3^-

465 (NO_3^-/ NO_2^* ratio) conversion efficiencies and the NH_3 concentration during the entire field

466 campaign (Fig.7). Note that only data points during nighttime (18 pm to 6 am) and with ambient

467 RH higher than 80% are displayed in Fig.8. Daytime data were excluded, because HONO would

468 quickly photolyze as soon as sunlight was available. Even if there was rapid HONO production,

469 the corresponding increase of HONO might not be observable due to its quick photolysis. The

470 reason for only including data with ambient RH higher than 80% is that the quick hydrolysis of

471 NO_2 requires water to be involved. However, the overall hygroscopicity of ambient aerosols during

472 this field campaign was relatively low, with an average hygroscopicity parameter κ of 0.14, and

473 the volume contribution of liquid water to the total volume concentrations of ambient aerosols was

474 quite low when ambient RH is below 80% (Kuang et al., 2018). The correlation coefficient between

475 HONO/NO_2^* ratio and the NH_3 concentration reaches 0.68, while that between NO_3^-/NO_2 ratio

476 and NH_3 concentration only reaches 0.53, since the source of NO_3^- is much more complicated than

477 that of HONO. These results have further verified that NH_3 promotes the NO_2 hydrolysis and

478 HONO production. The correlation of HONO/NO_2^* to NH_3 is highly nonlinear, HONO/NO_2^*

479 increases rapidly with NH_3 when NH_3 reaches above 10 ppb. In retrospect to Sect. 3 and Fig. 3, it

480 can be concluded that, under relatively cleaner conditions, the heterogeneous HONO formation
481 was mainly limited by particle surface area, while under polluted conditions, NH_3 concentration
482 was the dominant limiting factor.

483

484 **4.3 Feedback between HONO formation and inorganic secondary aerosol formation**

485 According to the discussions in Sect.4.2, NH_3 promotes the hydrolysis of NO_2, producing
486 nitrate and most of the observed HONO. However, the connection between the NH_3 promoted
487 hydrolysis and the simultaneous rapid sulfate production remains unexplained. As was already
488 discussed in Sect.4.2, the sulfate production rate calculated based on currently known SO_2
489 oxidation pathways largely underestimates the observed sulfate growth, indicating that there might
490 be neglected oxidation pathways. Li et al. (2018b) pointed out that NO_2 can oxidize S(IV)
491 indirectly via free radical mechanism (the involved reactions RS1 to RS5 proposed in Li et al.
492 (2018b) listed in the supplement). The key step of the proposed S(IV) oxidation pathway is the
493 photolysis of HONO to produce OH radicals (RS1). OH can oxidize S(IV) to form bisulfate or
494 sulfate through reaction RS2 and produce HO_2. HO_2 can react with NO to produce NO_2, or react
495 with itself to produce H_2O_2. As was depicted in Fig.6, the radiation during the fog/haze events was
496 already strong enough to photolyze the produced HONO and release OH radicals at the same rates
497 as L_{pho} in Sect. 4.1, indicating there was strong OH production, especially near the end of the
498 events. For the two fog events, no AOD measurements were available. Assuming AOD=2.5 for
499 foggy conditions, the lifetime of HONO (only considering the photolysis process) were estimated
500 to decrease from 4.2 to 1.1 h, 1.7 to 1.1 h during the growth of HONO and to drop to 1.0 and 0.7 h
501 by the time of the drastic decreases in HONO. In the haze event on the 11th Nov., AOD
502 measurements were also not available due to cloud coverage, however, sensitivity study shows
503 that the calculated HONO lifetime are much more sensitive to the AOD as opposed to the COD
504 values (increasing 3.1 and 0.4 h per 0.1 increase in AOD and COD, Fig.S7). The HONO lifetime
505 dropped from 2.0 h (by the time of the HONO peak) to 1.1 h (by time of the HONO decrease).
506 During the case on the 14th Nov. 2016, the relative humidity decreased from 100% (10:00-11:00)
507 to 86% (11:30), suggesting that this was a fog dissipation process. The HONO lifetime was
508 estimated to be 1.7 h between 10:00 to 11:00, proving that the photolysis process was relatively
509 weaker during the rapid increase of HONO. The estimated HONO lifetime rapidly decreased to
510 0.6 h by 12:00, resulting in accelerated HONO dissociation and OH production. The increase in

511 H_2O_2 observed during and after the increase of HONO, might be an indirect evidence of the HO_2

512 production and occurrence of RS2. The observed H_2O_2 concentrations were much higher than the

513 assumptions of 0.01 ppb made in Cheng et al. (2016), which was also pointed out by Ye et al.

514 (2018). Under the assumed pH range for fog and the calculated pH range for aerosol, the estimated

515 sulfate production was dominated by the SO_2 oxidation via H_2O_2 (Fig.7). This indicates that both

516 the calculated and the yet unexplained sulfate production were linked to the photolysis of HONO.

517   NH_3 promoted the hydrolysis of NO_2, producing HONO and nitrate. HONO easily photolyzes

518 releasing OH radicals, which further converted to HO_2 and H_2O_2. The highly oxidative free radicals

519 and H_2O_2 collaboratively boosted the formation of sulfate. Hence, diurnal variations of NH_3 should

520 have exerted significant influences on the diurnal variations of HONO and inorganic aerosol

521 chemical components (sulfate, nitrate and ammonium, SNA). The average diurnal variations of

522 NO_2^*, NH_3, HONO as well as SO_2 concentrations during this field campaign are shown in Fig.9a.

523 The average HONO concentration during nighttime is higher than that during daytime due to the

524 quick photolysis of HONO upon solar irradiation. The NH_3 concentration begins to increase in the

525 morning (near 8:00 LT) the reaches a plateau in the afternoon (8.5 to 15.5 ppb in average), and the

526 SO_2 concentrations shows a similar diurnal variation to that of NH_3. This type of diurnal variation

527 of SO_2 was also found by Xu et al. (2014), however, the cause of the common diurnal pattern

528 between NH_3 and SO_2 during this field campaign requires further investigation. The NO_2^*

529 concentration increases quickly in the afternoon and decreases in the evening.

530   As shown in Fig.9b, the increase of NH_3 from morning to the afternoon was accompanied

531 with the increase of mass fractions of nitrate and sulfate in $PM_{2.5}$ (The mass fractions of different

532 aerosol chemical compositions were obtained by using the measured dry state PNSD to calculate

533 volume concentration of $PM_{2.5}$, assuming that the density of aerosols in dry state is 1.5 g cm^{-3} (Yin

534 et al., 2015). The results shown in Fig.9b indicate that the molecular concentration increase in

535 nitrate from the morning to the afternoon is much faster than that of sulfate, again supporting the

536 fact that the NH_3-promoted NO_2 hydrolysis, which only produces HONO and nitrate directly, was

537 the main contributor to the observed explosive HONO formation. The evident morning increase

538 of inorganic aerosol component fractions resulted in prominent increases of aerosol hygroscopicity,

539 displaying an average κ anomaly of +0.04 during noontime (Fig.9c). From the morning to the

540 afternoon, the ambient RH decreases quickly, however, the increase of aerosol hygroscopicity can

541 retard the decrease of aerosol liquid water content and surface area density of ambient aerosols.

542   This might act as a positive feedback, further enhancing the hydrolysis of NO_2 as well as the nitrate

543   and sulfate formation.

544   **5. Summary and atmospheric implications**

545   Explosive HONO growth (observed maximum d[HONO]/dt=16.1 ppb h^{-1}) was observed

546   for the first time on the NCP during fog and haze episodes with high RH conditions, only occurring

547   with evident increases in NH_3, indicating that NH_3 is the key factor promoting the hydrolysis of

548   NO_2, resulting in rapid HONO and nitrate formation. NH_3 concentrations during the observation

549   period exhibit a distinct diurnal variation with an increase in the morning and a peak in the

550   afternoon (8.5 to 15.5 ppb in average). The increase of NH_3 promotes the hydrolysis of NO_2, giving

551   significant rise to HONO and nitrate concentrations. Produced HONO released OH radicals upon

552   photolysis, which further oxidized SO_2 to sulfate through gas phase and heterogeneous reactions.

553   Therefore, the significant growth of NH_3 in the morning determined the increase in nitrate, sulfate

554   and ammonium as well as that of aerosol hygroscopicity, which as a positive feedback retards the

555   decrease in atmospheric liquid water content and further enhances the hydrolysis of NO_2 as well

556   as the nitrate and sulfate formation.

557   Results in this paper reveals that the NH_3-promoted NO_2 hydrolysis is a significant source

558   of HONO, especially under polluted conditions, which provides direct insight into the missing

559   daytime source of HONO on the NCP. Results in this paper also shed light on the recent

560   controversy of how SO_2, pH and NH_3 are involved in heterogeneous HONO production. It was

561   clarified that in the HONO production, SO_2 took a minor part during fog events and an insignificant

562   part during haze events, the observed growth in sulfate was dominantly the byproduct of the

563   HONO photolysis, confirming again the importance HONO as an OH source and its crucial role

564   in atmospheric chemistry.

565   These results have demonstrated the critical role and contribution of NH_3 in the formation

566   of photochemical and aerosol pollution on the North China Plain. Effective control measures are

567   urgently called for to reduce NH_3 emissions, which would simultaneously benefit the

568   photochemical and aerosol pollution abatement through the reduction of HONO production.

569   **Author contribution**

570   WX designed the experiment and YK led the research. YK, JT, GZ, YB, YY, CS and LL
571   were responsible for the aerosol measurements in the experiment, WY helped with the IGAC
572   measurements. WX made the trace gas measurements with the help of ZG, WL and XX. YK and
573   WX analyzed the data and wrote the paper.

574

Acknowledgments, Samples, and Data

This work is supported by the National Key R&D Program of China (2016YFC0202300), the National research program for key issues in air pollution control (DQGG0103) and the National Natural Science Foundation of China (41505107 and 41590872). We thank Wei Peng from Beijing Met High-Tech Co., Ltd. for his help with the maintenance of the IGAC instrument.

Data availability. The data used in this study are available from the corresponding author upon request (kuangye@jnu.edu.cn)

References

Cheng, Y., Zheng, G., Wei, C., Mu, Q., Zheng, B., Wang, Z., Gao, M., Zhang, Q., He, K., Carmichael, G., Pöschl, U., and Su, H.: Reactive nitrogen chemistry in aerosol water as a source of sulfate during haze events in China, Science Advances, 2, e1601530, 10.1126/sciadv.1601530, 2016.

Cui, L., Li, R., Zhang, Y., Meng, Y., Fu, H., and Chen, J.: An observational study of nitrous acid (HONO) in Shanghai, China: The aerosol impact on HONO formation during the haze episodes, Science of The Total Environment, 630, 1057-1070, https://doi.org/10.1016/j.scitotenv.2018.02.063, 2018.

Ding, J., Zhao, P., Su, J., Dong, Q., and Du, X.: Aerosol pH and its influencing factors in Beijing, Atmos. Chem. Phys. Discuss., 2018, 1-34, 10.5194/acp-2018-270, 2018.

Guo, H., Weber, R. J., and Nenes, A.: High levels of ammonia do not raise fine particle pH sufficiently to yield nitrogen oxide-dominated sulfate production, Scientific reports, 7, 12109, 10.1038/s41598-017-11704-0, 2017.

Huang, R.-J., Yang, L., Cao, J., Wang, Q., Tie, X., Ho, K.-F., Shen, Z., Zhang, R., Li, G., Zhu, C., Zhang, N., Dai, W., Zhou, J., Liu, S., Chen, Y., Chen, J., and O'Dowd, C. D.: Concentration and sources of atmospheric nitrous acid (HONO) at an urban site in Western China, Science of The Total Environment, 593-594, 165-172, https://doi.org/10.1016/j.scitotenv.2017.02.166, 2017.

Kleffmann, J., Gavriloaiei, T., Hofzumahaus, A., Holland, F., Koppmann, R., Rupp, L., Schlosser, E., Siese, M., and Wahner, A.: Daytime formation of nitrous acid: A major source of OH radicals in a forest, Geophysical Research Letters, 32, doi:10.1029/2005GL022524, 2005.

Kuang, Y., Zhao, C. S., Tao, J. C., and Ma, N.: Diurnal variations of aerosol optical properties in the North China Plain and their influences on the estimates of direct aerosol radiative forcing, Atmos. Chem. Phys. Discuss., 15, 339-369, 10.5194/acpd-15-339-2015, 2015.

Kuang, Y., Zhao, C., Tao, J., Bian, Y., Ma, N., and Zhao, G.: A novel method for deriving the aerosol hygroscopicity parameter based only on measurements from a humidified nephelometer system, Atmos. Chem. Phys., 17, 6651-6662, 10.5194/acp-17-6651-2017, 2017.

Kuang, Y., Zhao, C. S., Zhao, G., Tao, J. C., Xu, W., Ma, N., and Bian, Y. X.: A novel method for calculating ambient aerosol liquid water content based on measurements of a humidified nephelometer system, Atmospheric Measurement Techniques, 11, 2967-2982, 10.5194/amt-11-2967-2018, 2018.

Li, G., Lei, W., Zavala, M., Volkamer, R., Dusanter, S., Stevens, P., and Molina, L. T.: Impacts of HONO sources on the photochemistry in Mexico City during the MCMA-2006/MILAGO Campaign, Atmos. Chem. Phys., 10, 6551-6567, 10.5194/acp-10-6551-2010, 2010.

Li, L., Duan, Z., Li, H., Zhu, C., Henkelman, G., Francisco, J. S., and Zeng, X. C.: Formation of HONO from the NH3-promoted hydrolysis of NO2-dimers in the atmosphere, Proceedings of the National Academy of Sciences, 10.1073/pnas.1807719115, 2018a.

Li, L., Hoffmann, M. R., and Colussi, A. J.: Role of Nitrogen Dioxide in the Production of Sulfate during Chinese Haze-Aerosol Episodes, Environmental Science & Technology, 52, 2686-2693, 10.1021/acs.est.7b05222, 2018b.

Li, X., Brauers, T., Häseler, R., Bohn, B., Fuchs, H., Hofzumahaus, A., Holland, F., Lou, S., Lu, K. D., Rohrer, F., Hu, M., Zeng, L. M., Zhang, Y. H., Garland, R. M., Su, H., Nowak, A., Wiedensohler, A., Takegawa, N., Shao, M., and Wahner, A.: Exploring the atmospheric chemistry of nitrous acid (HONO) at a rural site in Southern China, Atmospheric Chemistry and Physics, 12, 1497-1513, 10.5194/acp-12-1497-2012, 2012.

Liu, M., Song, Y., Zhou, T., Xu, Z., Yan, C., Zheng, M., Wu, Z., Hu, M., Wu, Y., and Zhu, T.: Fine particle pH during severe haze episodes in northern China, Geophysical Research Letters, 44, 5213-5221, doi:10.1002/2017GL073210, 2017a.

Liu, Y., Wu, Z., Wang, Y., Xiao, Y., Gu, F., Zheng, J., Tan, T., Shang, D., Wu, Y., Zeng, L., Hu, M., Bateman, A. P., and Martin, S. T.: Submicrometer Particles Are in the Liquid State during Heavy Haze Episodes in the Urban Atmosphere of Beijing, China, Environmental Science & Technology Letters, 4, 427-432, 10.1021/acs.estlett.7b00352, 2017b.

Liu, Z., Wang, Y., Costabile, F., Amoroso, A., Zhao, C., Huey, L. G., Stickel, R., Liao, J., and Zhu, T.: Evidence of Aerosols as a Media for Rapid Daytime HONO Production over China, Environmental Science & Technology, 48, 14386-14391, 10.1021/es504163z, 2014.

Lu, C., Niu, S., Tang, L., Lv, J., Zhao, L., and Zhu, B.: Chemical composition of fog water in Nanjing area of China and its related fog microphysics, Atmospheric Research, 97, 47-69, http://dx.doi.org/10.1016/j.atmosres.2010.03.007, 2010.

Lu, K., Guo, S., Tan, Z., Wang, H., Shang, D., Liu, Y., Li, X., Wu, Z., Hu, M., and Zhang, Y.: Exploring atmospheric free-radical chemistry in China: the self-cleansing capacity and the formation of secondary air pollution, National Science Review, nwy073-nwy073, 10.1093/nsr/nwy073, 2018.

Meng, Z., Xu, X., Lin, W., Ge, B., Xie, Y., Song, B., Jia, S., Zhang, R., Peng, W., Wang, Y., Cheng, H., Yang, W., and Zhao, H.: Role of ambient ammonia in particulate ammonium formation at a rural site in the North China Plain, Atmos. Chem. Phys., 18, 167-184, 10.5194/acp-18-167-2018, 2018.

Michoud, V., Colomb, A., Borbon, A., Miet, K., Beekmann, M., Camredon, M., Aumont, B., Perrier, S., Zapf, P., Siour, G., Ait-Helal, W., Afif, C., Kukui, A., Furger, M., Dupont, J. C., Haeffelin, M., and Doussin, J. F.: Study of the unknown HONO daytime source at a European suburban site during the MEGAPOLI summer and winter field campaigns, Atmos. Chem. Phys., 14, 2805-2822, 10.5194/acp-14-2805-2014, 2014.

Nie, W., Ding, A. J., Xie, Y. N., Xu, Z., Mao, H., Kerminen, V. M., Zheng, L. F., Qi, X. M., Huang, X., Yang, X. Q., Sun, J. N., Herrmann, E., Petäjä, T., Kulmala, M., and Fu, C. B.: Influence of biomass burning plumes on HONO chemistry in eastern China, Atmos. Chem. Phys., 15, 1147-1159, 10.5194/acp-15-1147-2015, 2015.

Petters, M. D., and Kreidenweis, S. M.: A single parameter representation of hygroscopic growth and cloud condensation nucleus activity, Atmospheric Chemistry and Physics, 7, 1961-1971, 2007.

Ran, L., Zhao, C. S., Xu, W. Y., Lu, X. Q., Han, M., Lin, W. L., Yan, P., Xu, X. B., Deng, Z. Z., Ma, N., Liu, P. F., Yu, J., Liang, W. D., and Chen, L. L.: VOC reactivity and its effect on ozone production during the HaChi summer campaign, Atmos. Chem. Phys., 11, 4657-4667, 10.5194/acp-11-4657-2011, 2011.

Safai, P. D., Kewat, S., Pandithurai, G., Praveen, P. S., Ali, K., Tiwari, S., Rao, P. S. P., Budhawant, K. B., Saha, S. K., and Devara, P. C. S.: Aerosol characteristics during winter fog at Agra, North India, J. Atmos. Chem., 61, 101-118, 10.1007/s10874-009-9127-4, 2008.

Shao, J., Chen, Q., Wang, Y., Lu, X., He, P., Sun, Y., Shah, V., Martin, R. V., Philip, S., Song, S., Zhao, Y., Xie, Z., Zhang, L., and Alexander, B.: Heterogeneous sulfate aerosol formation mechanisms during wintertime Chinese haze events: Air quality model assessment using observations of sulfate oxygen isotopes in Beijing, Atmos. Chem. Phys. Discuss., 2019, 1-28, 10.5194/acp-2018-1352, 2019.

Shen, C., Zhao, C., Ma, N., Tao, J., Zhao, G., Yu, Y., and Kuang, Y.: Method to Estimate Water Vapor Supersaturation in the Ambient Activation Process Using Aerosol and Droplet Measurement Data, Journal of Geophysical Research: Atmospheres, 123, 10606-10619, doi:10.1029/2018JD028315, 2018.

Song, S., Gao, M., Xu, W., Shao, J., Shi, G., Wang, S., Wang, Y., Sun, Y., and McElroy, M. B.: Fine-particle pH for Beijing winter haze as inferred from different thermodynamic equilibrium models, Atmos. Chem. Phys., 18, 7423-7438, 10.5194/acp-18-7423-2018, 2018.

Stutz, J., Alicke, B., and Neftel, A.: Nitrous acid formation in the urban atmosphere: Gradient measurements of NO2 and HONO over grass in Milan, Italy, Journal of Geophysical Research: Atmospheres, 107, LOP 5-1-LOP 5-15, doi:10.1029/2001JD000390, 2002.

Su, H., Cheng, Y., Oswald, R., Behrendt, T., Trebs, I., Meixner, F. X., Andreae, M. O., Cheng, P., Zhang, Y., and Pöschl, U.: Soil Nitrite as a Source of Atmospheric HONO and OH Radicals, Science, 333, 1616-1618, 10.1126/science.1207687, 2011.

Teng, X., Hu, Q., Zhang, L., Qi, J., Shi, J., Xie, H., Gao, H., and Yao, X.: Identification of Major Sources of Atmospheric NH3 in an Urban Environment in Northern China During Wintertime, Environmental Science & Technology, 51, 6839-6848, 10.1021/acs.est.7b00328, 2017.

Vogel, B., Vogel, H., Kleffmann, J., and Kurtenbach, R.: Measured and simulated vertical profiles of nitrous acid—Part II. Model simulations and indications for a photolytic source, Atmospheric Environment, 37, 2957-2966, https://doi.org/10.1016/S1352-2310(03)00243-7, 2003.

Wang, G., Zhang, R., Gomez, M. E., Yang, L., Levy Zamora, M., Hu, M., Lin, Y., Peng, J., Guo, S., Meng, J., Li, J., Cheng, C., Hu, T., Ren, Y., Wang, Y., Gao, J., Cao, J., An, Z., Zhou, W., Li, G., Wang, J., Tian, P., Marrero-Ortiz, W., Secrest, J., Du, Z., Zheng, J., Shang, D., Zeng, L., Shao, M., Wang, W., Huang, Y., Wang, Y., Zhu, Y., Li, Y., Hu, J., Pan, B., Cai, L., Cheng, Y., Ji, Y., Zhang, F., Rosenfeld, D., Liss, P. S., Duce, R. A., Kolb, C. E., and Molina, M. J.: Persistent sulfate formation from London Fog to Chinese haze, Proceedings of the National Academy of Sciences, 10.1073/pnas.1616540113, 2016.

Whalley, L. K., Stone, D., George, I. J., Mertes, S., van Pinxteren, D., Tilgner, A., Herrmann, H., Evans, M. J., and Heard, D. E.: The influence of clouds on radical concentrations: observations and modelling studies of HO$_x$ during the Hill Cap Cloud Thuringia (HCCT) campaign in 2010, Atmos. Chem. Phys., 15, 3289-3301, 10.5194/acp-15-3289-2015, 2015.

Wu, Z., Wang, Y., Tan, T., Zhu, Y., Li, M., Shang, D., Wang, H., Lu, K., Guo, S., Zeng, L., and Zhang, Y.: Aerosol Liquid Water Driven by Anthropogenic Inorganic Salts: Implying Its Key Role in Haze Formation over the North China Plain, Environmental Science & Technology Letters, 10.1021/acs.estlett.8b00021, 2018.

Xing, J., Ding, D., Wang, S., Zhao, B., Jang, C., Wu, W., Zhang, F., Zhu, Y., and Hao, J.: Quantification of the enhanced effectiveness of NOx control from simultaneous reductions of VOC and NH3 for reducing air pollution in the Beijing–Tianjin–Hebei region, China, Atmos. Chem. Phys., 18, 7799-7814, 10.5194/acp-18-7799-2018, 2018.

Xu, W. Y., Zhao, C. S., Ran, L., Lin, W. L., Yan, P., and Xu, X. B.: SO2 noontime-peak phenomenon in the North China Plain, Atmospheric Chemistry and Physics, 14, 7757-7768, 10.5194/acp-14-7757-2014, 2014.

Xue, L. K., Wang, T., Gao, J., Ding, A. J., Zhou, X. H., Blake, D. R., Wang, X. F., Saunders, S. M., Fan, S. J., Zuo, H. C., Zhang, Q. Z., and Wang, W. X.: Ground-level ozone in four Chinese cities: precursors, regional transport and heterogeneous processes, Atmos. Chem. Phys., 14, 13175-13188, 10.5194/acp-14-13175-2014, 2014.

Yabushita, A., Enami, S., Sakamoto, Y., Kawasaki, M., Hoffmann, M. R., and Colussi, A. J.: Anion-Catalyzed Dissolution of NO2 on Aqueous Microdroplets, The Journal of Physical Chemistry A, 113, 4844-4848, 10.1021/jp900685f, 2009.

Ye, C., Liu, P., Ma, Z., Xue, C., Zhang, C., Zhang, Y., Liu, J., Liu, C., Sun, X., and Mu, Y.: High H2O2 Concentrations Observed during Haze Periods during the Winter in Beijing: Importance of H2O2 Oxidation in Sulfate Formation, Environmental Science & Technology Letters, 10.1021/acs.estlett.8b00579, 2018.

Yin, Z., Ye, X., Jiang, S., Tao, Y., Shi, Y., Yang, X., and Chen, J.: Size-resolved effective density of urban aerosols in Shanghai, Atmospheric Environment, 100, 133-140, http://dx.doi.org/10.1016/j.atmosenv.2014.10.055, 2015.

Young, L.-H., Li, C.-H., Lin, M.-Y., Hwang, B.-F., Hsu, H.-T., Chen, Y.-C., Jung, C.-R., Chen, K.-C., Cheng, D.-H., Wang, V.-S., Chiang, H.-C., and Tsai, P.-J.: Field performance of a semi-continuous monitor for ambient PM2.5 water-soluble inorganic ions and gases at a suburban site, Atmospheric Environment, 144, 376-388, https://doi.org/10.1016/j.atmosenv.2016.08.062, 2016.

Zhang, W., Tong, S., Ge, M., An, J., Shi, Z., Hou, S., Xia, K., Qu, Y., Zhang, H., Chu, B., Sun, Y., and He, H.: Variations and sources of nitrous acid (HONO) during a severe pollution episode in Beijing in winter 2016, Science of The Total Environment, 648, 253-262, https://doi.org/10.1016/j.scitotenv.2018.08.133, 2019.

Zheng, G. J., Duan, F. K., Su, H., Ma, Y. L., Cheng, Y., Zheng, B., Zhang, Q., Huang, T., Kimoto, T., Chang, D., Pöschl, U., Cheng, Y. F., and He, K. B.: Exploring the severe winter haze in Beijing: the impact of synoptic weather, regional transport and heterogeneous reactions, Atmos. Chem. Phys., 15, 2969-2983, 10.5194/acp-15-2969-2015, 2015.
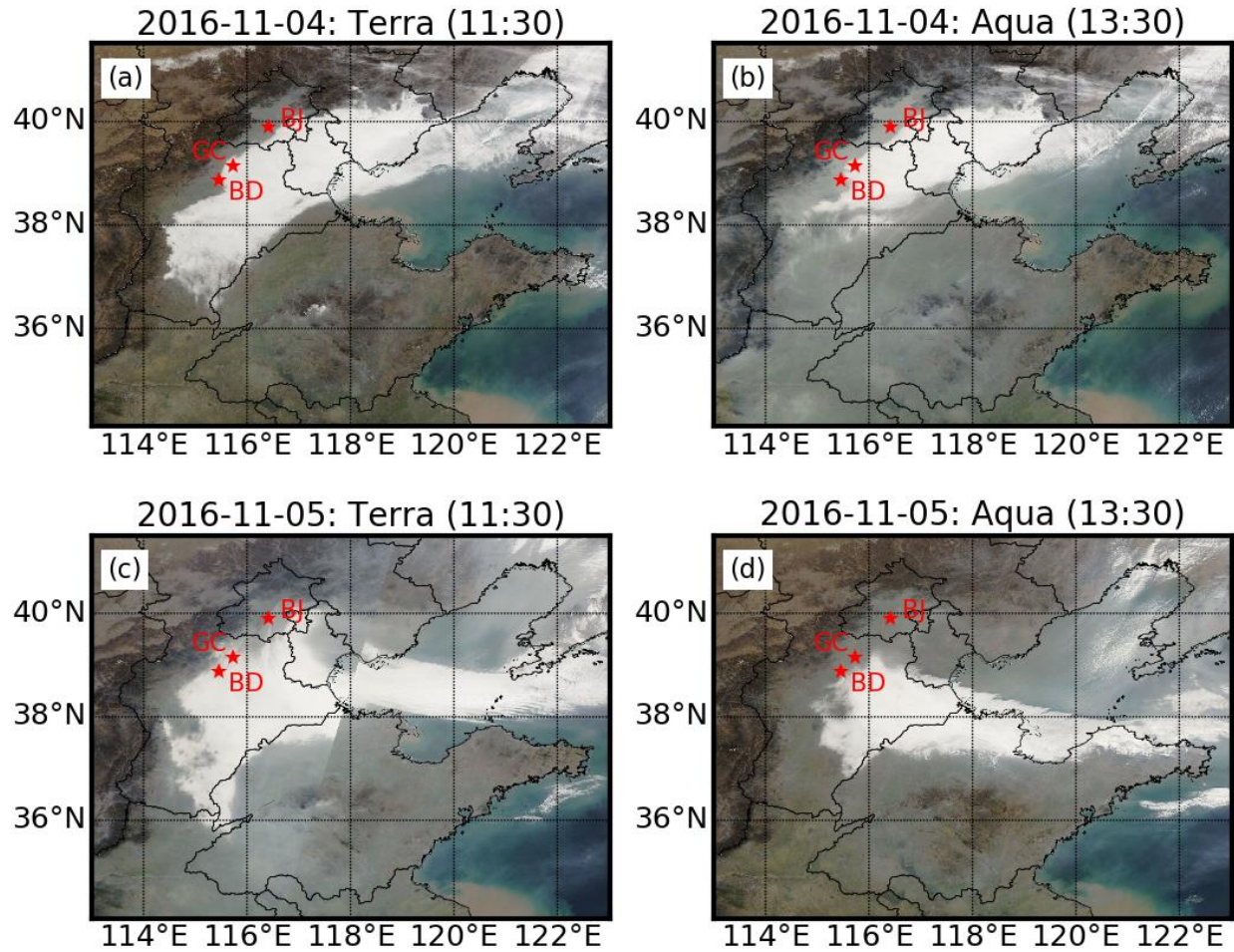
747
748 **Figure 1**. MODIS Terra (a,c) and Aqua (b,d) satellite images in 04th Nov. (a,b) and 5th Nov. 2016
749 (c,d), star markers are locations of Gucheng (GC: the observation site), Baoding (BD) and Beijing
750 (BJ).
751

752

753
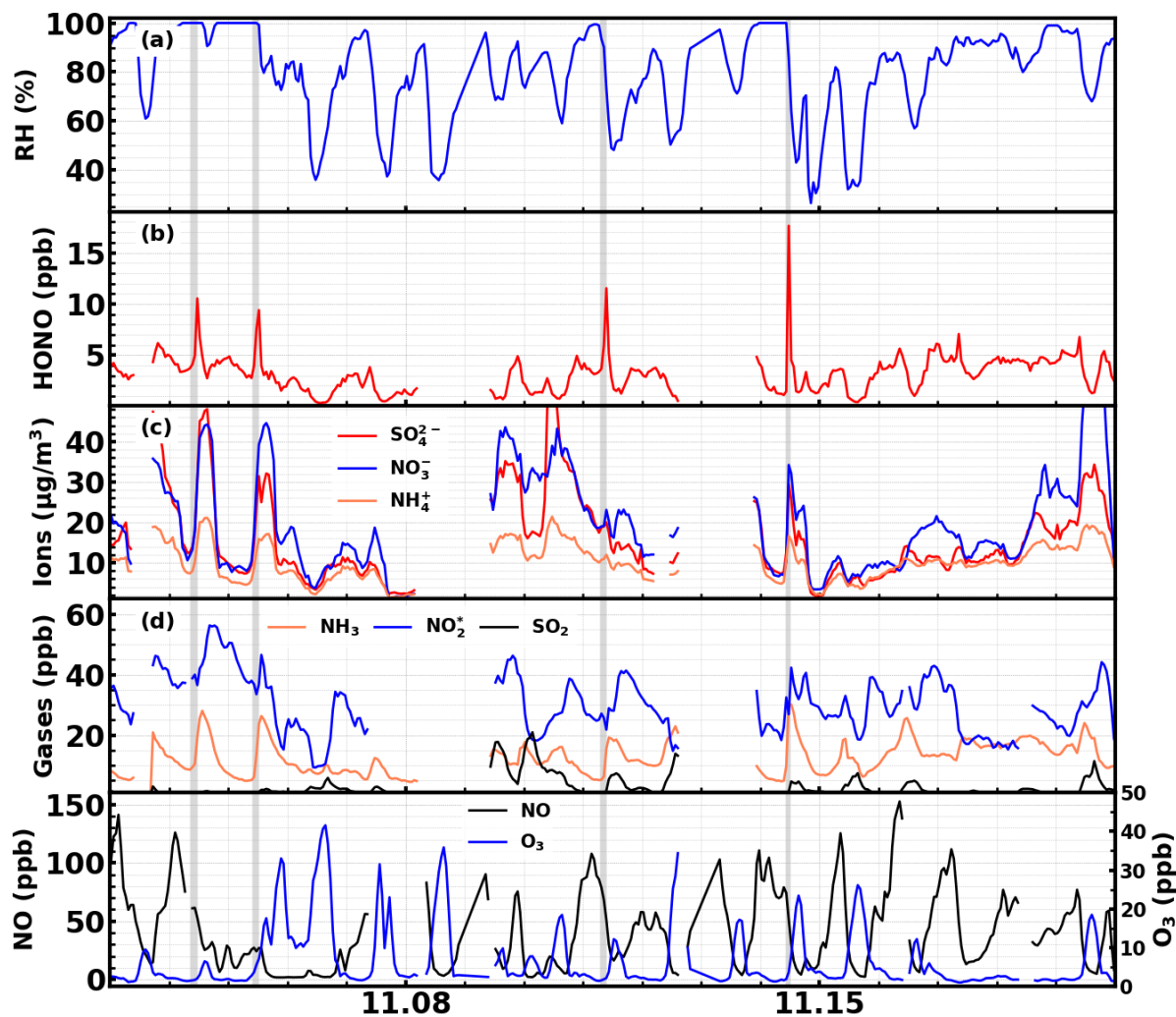
Figure 2. Time series of ambient **a)** RH; **b)** HONO; **c)** sulfate, nitrate, ammonium; **d)** NH_3, NO_2^*
and SO_2 during the observation period.

756
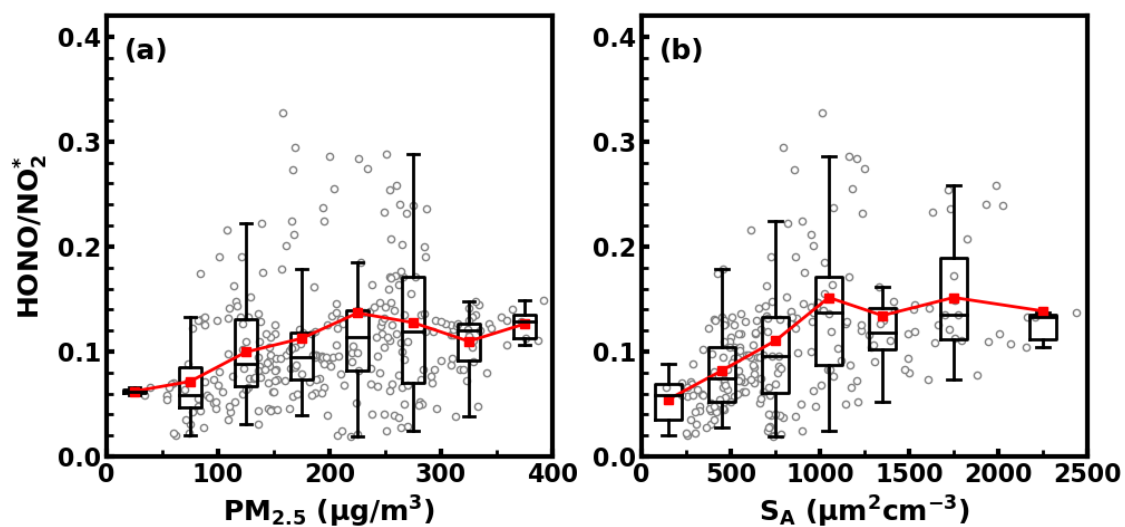
757
758 **Figure 3** Boxplots displaying the variation of HONO/NO$_2^*$ with a) PM$_{2.5}$ concentration and b)
759 ambient aerosol surface area density.
760
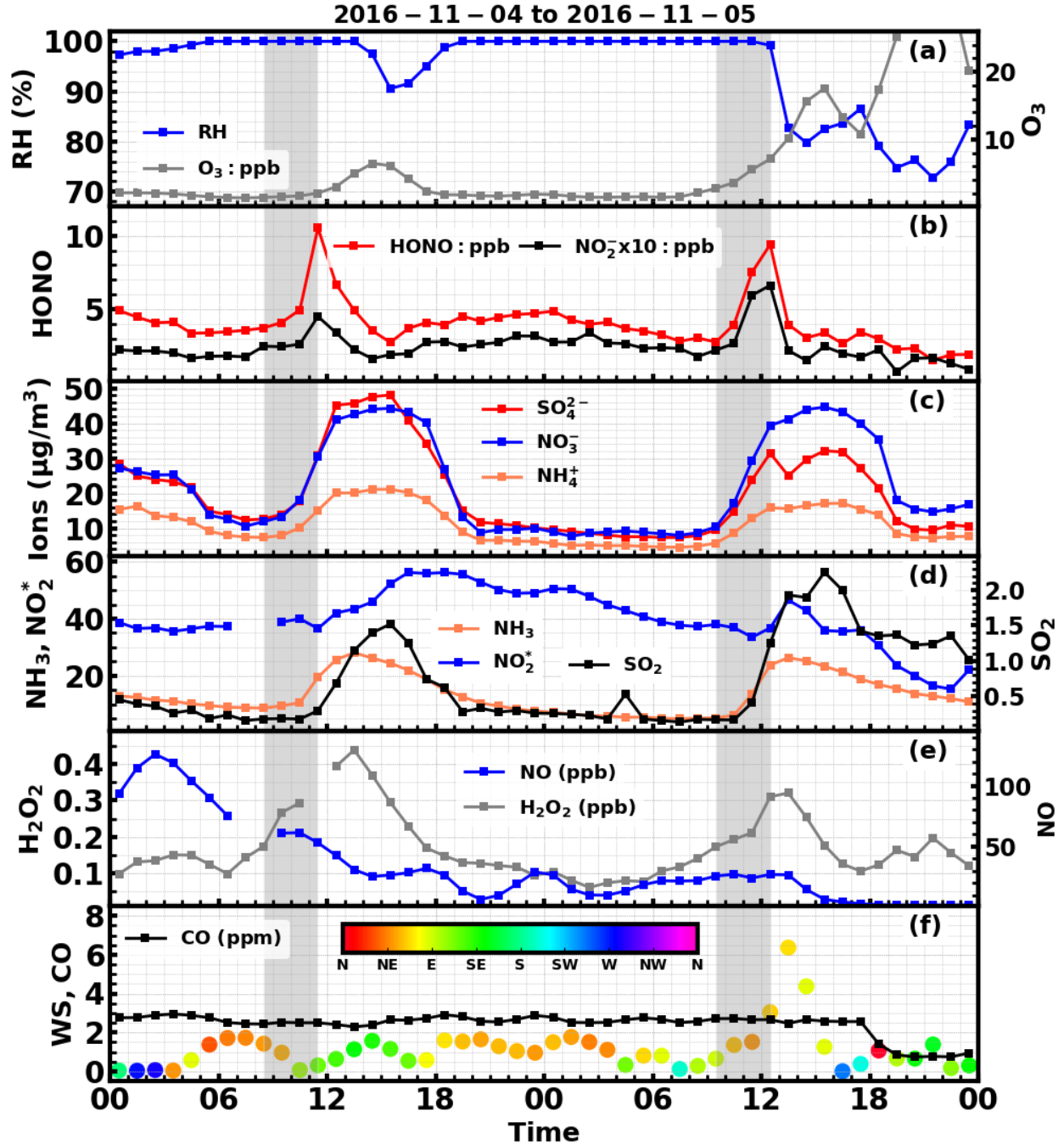
Figure 4 Time series of ambient **a)** RH,O_3, **b)**HONO, NO_2^-, **c)** SO_4^{2-}, NO_3^-, NH_4^+, **d)** NH$_3$, NO_2^*, SO$_2$, **e)** NO, H_2O_2, **f)** CO, wind speed and wind direction (colors of scatter points) from 4th to 5th Nov. 2016. Gray shaded areas represent periods of rapid increase of HONO.

766
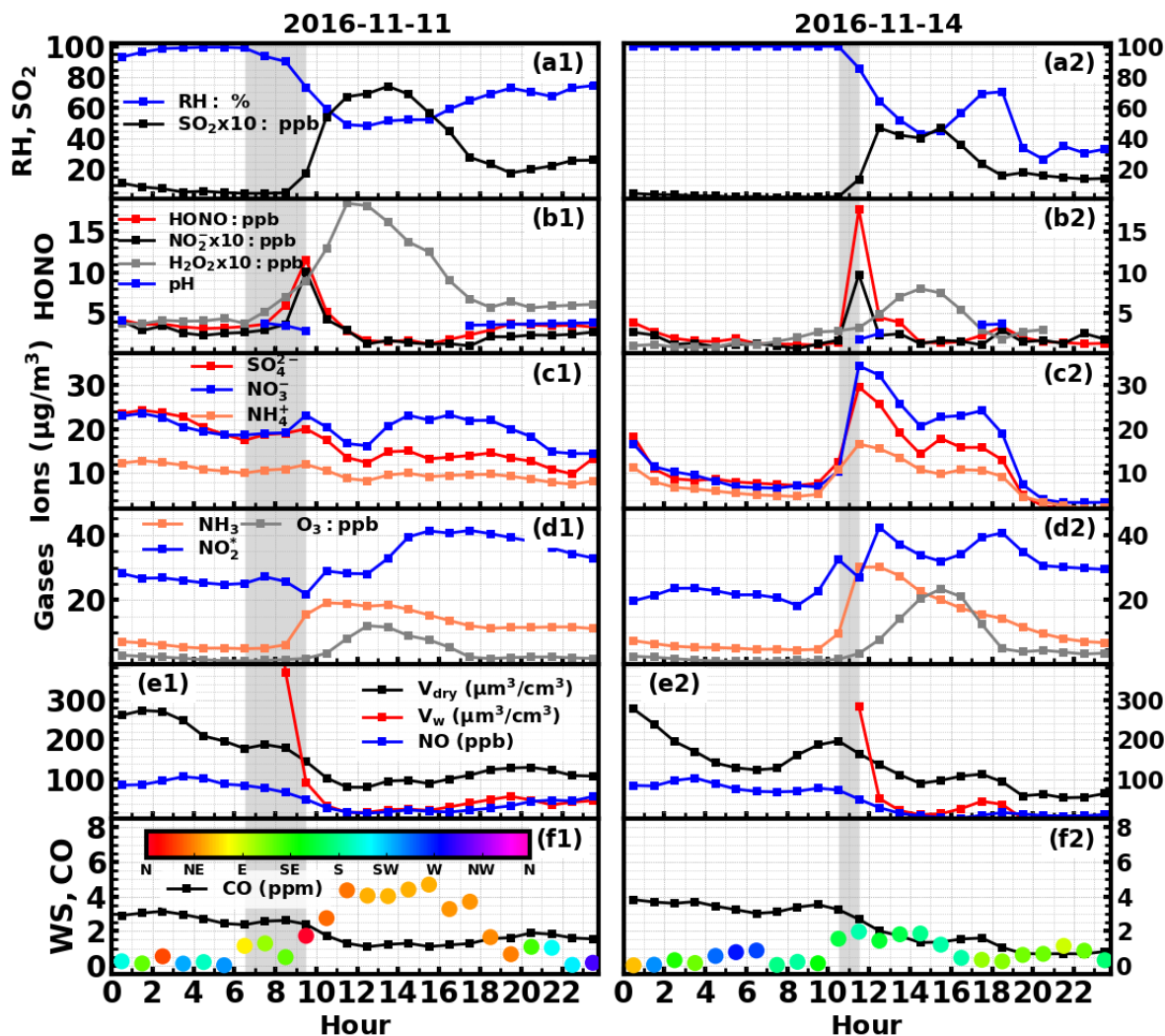
Figure 5 Time series of ambient **a)** RH, SO$_2$, **b)** HONO, NO$_2^-$, H$_2$O$_2$, aerosol pH, **c)** SO$_4^{2-}$, NO$_3^-$,
NH$_4^+$, **d)** NH$_3$, NO$_2^*$, O$_3$, **e)** NO, volume concentrations of PM$_{2.5}$ in dry state (V$_{dry}$), volume
concentrations of liquid water (V$_w$), **f)** CO, wind speed and wind direction during **1)** 11th Nov. 2016
and **2)** 14th Nov. 2016. Gray shaded areas represents periods of rapid increase of HONO.

771

772
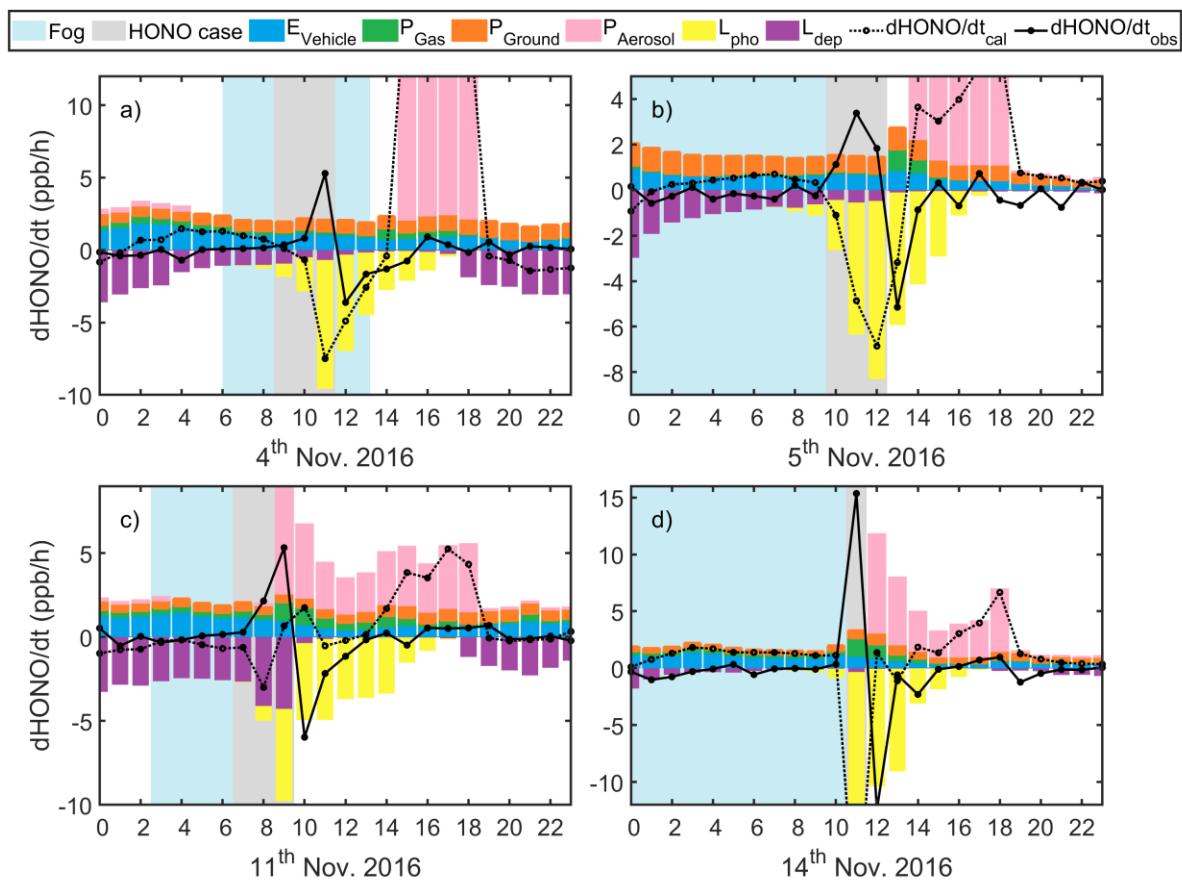
Figure 6 Estimated HONO emission from vehicles (blue), gas phase production (green), production on ground (orange) and aerosol surface (pink), loss through photolysis (yellow) and dry deposition (purple), as well as the calculated (dotted black) and actually observed (solid black) d[HONO]/dt on a) 4th, b) 5th, c) 11th and d) 14th Nov. 2016.

777
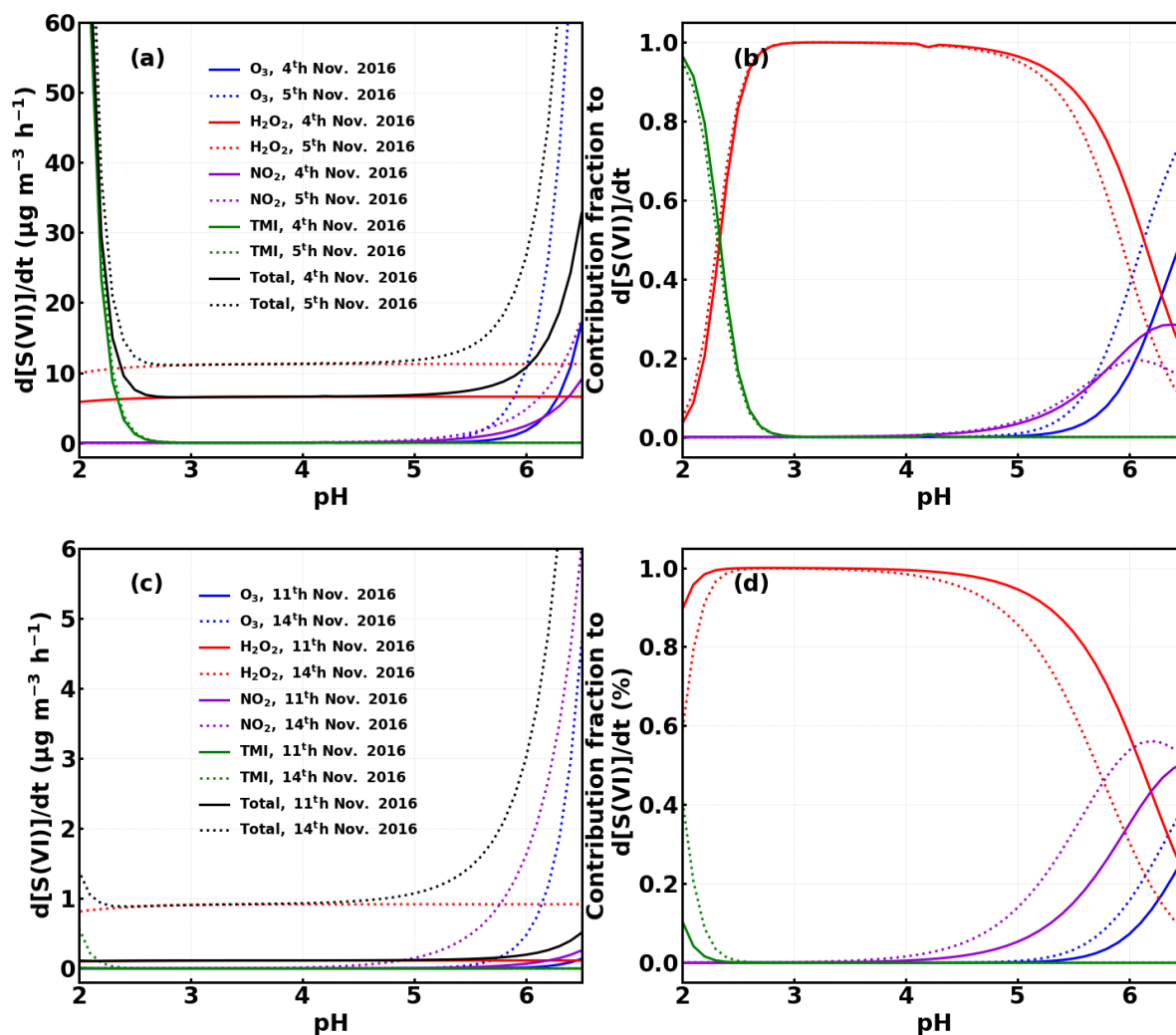
778
779 **Figure 7** Calculated average sulfate production (a,c) and contribution fraction b,d) from SO_2
780 oxidation by H_2O_2, NO_2^*, O_3, TMI under different pH values using methods described in (Cheng
781 et al., 2016) for the case episodes on 4th, 5th, 11th and 14th Nov. 2016.
782
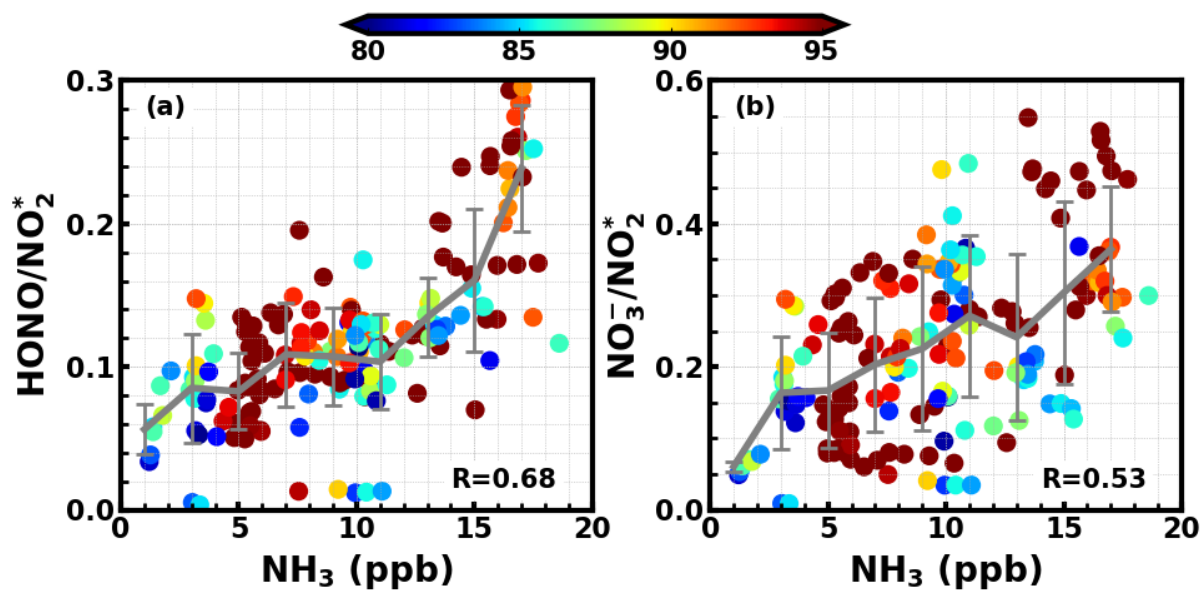
783
784 **Figure 8** The relationship between NH_3 concentration and **a)** HONO/ NO_2^* ratio; **b)**
785 nitrate/nitrogen dioxide ratio (NO_3^-/NO_2^*); Colors of scatter points represent ambient RHs and the
786 color bar is shown on the top.
787

788

789
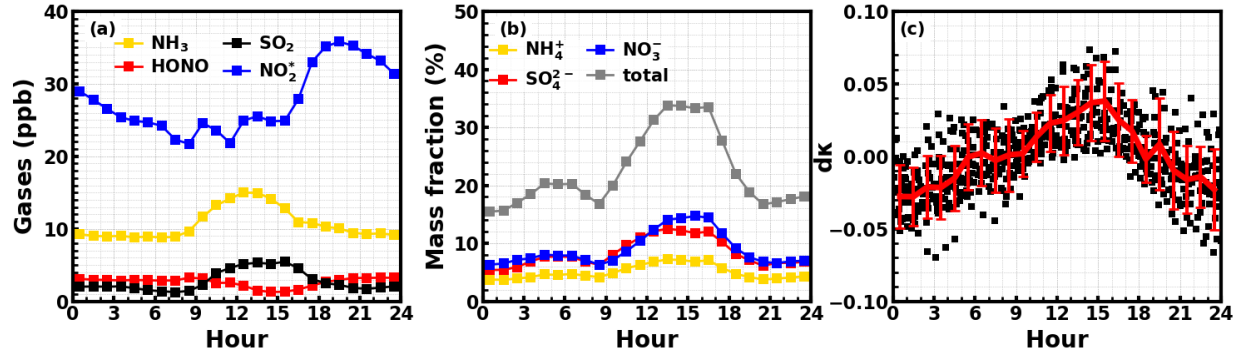
790 **Figure 9. (a)** Average diurnal variations of Gases; **(b)** Average diurnal variations of mass
791 fractions **of** nitrate, sulfate and ammonium; **(c)** Diurnal variations of aerosol hygroscopicity, dκ is
792 the anomaly to the daily mean κ.